

Numerical formulation of three-dimensional scattering problems for optical structures

Tatsuya Usuki*

*Institute for Photonics-Electronics Convergence System Technology (PECST),
Photonics Electronics Technology Research Association (PETRA),
West 7 SCR, 16-1 Onogawa, Tsukuba, Ibaraki 305-8569*

(Dated: February 21, 2013)

This paper describes a numerical formulation for calculating wave propagation with high precision in a three-dimensional system. Yee's discretization scheme is used to formulate a frequency domain method that is compatible with the finite-difference time-domain (FDTD) procedure. When the S-matrix satisfies a unitarity (power flow conservation) condition, the method enables arbitrary S-matrix elements to be obtained within a numerical error of less than 10^{-8} (2×10^{-13}) for double precision format.

PACS numbers: 02.60.Cb, 41.20.Jb, 42.15.Eq, 42.25.Bs

I. INTRODUCTION

Numerical simulations are important for studying electromagnetic-wave propagation in optical physics [1] and for designing silicon photonics [2, 3]. One of the most successful numerical methods is the finite-difference time-domain (FDTD) method [4]. It is suitable for visualizing dynamical propagation of electromagnetic waves. Simulations should not only give us a general understanding of the propagation, but also the details of the optical scattering.

Designing chips such as silicon optical interposers [5] requires highly precise simulations including the transmittance and reflectance of the fundamental and higher order modes at each wavelength (i.e., each frequency). Small reflections may cause substantial instability [6] between devices on the optical chip, and the small losses that result may build up (e.g. see Table I in Ref. [5]). Thus, we need a way to confirm that the numerical results are precise when the scattering properties are simulated.

Here, we should note that the precision of a numerical calculation, which is affected by both numerical method (e.g. numerical stability for the FDTD [7]) and numerical implementation (e.g. floating-point arithmetic [8]), is essentially different from the accuracy of numerical modeling that includes both the choice of the fundamental equation (e.g. microscopic nonlocal approach [9] is one such choice) and the discretization of the numerical procedure (e.g. numerical dispersion for the FDTD [7]). In a scattering simulation, the error related to the accuracy is often explicit and predictable, but the error related to the precision is apt to be implicit and unforeseeable. The S-matrix approach [10] is widely used to study scattering problems [11], and numerical S-matrices have already been applied to scattering simulations on photonic crystal slabs [12–14] and metal films [15]. Unfortunately, no

method as yet has been discussed related to highly precise simulations in the three-dimensional optical structures.

This paper proposes a numerical method that can produce precise S-matrices for designing the silicon photonics devices. The method exploits a numerical procedure for quantum transport [16, 17]. The numerical precision of the method is evaluated in terms of the S-matrix properties.

II. FORMULATION

Consider the macroscopic Maxwell equations in the angular frequency domain (ω space),

$$\begin{aligned}\nabla \times \mathbf{H} &= -i\omega\epsilon_0\epsilon(\mathbf{x})\mathbf{E}, \\ \nabla \times \mathbf{E} &= i\omega\mu_0\mu(\mathbf{x})\mathbf{H},\end{aligned}\tag{1}$$

where ϵ_0 (μ_0) is vacuum permittivity (permeability). The symbol i denotes an imaginary number, and the notation “ $\exp(-i\omega t)$ ” describes a harmonic oscillation. The symbols j , k , l , m , and n in the following formulation denote integers. Instead of using dipole moments in the optical media, Eqs. (1) are used to express the relative permittivity $\epsilon(\mathbf{x})$ and relative permeability $\mu(\mathbf{x})$. Note that $\text{Im}\epsilon(\mathbf{x}), \text{Im}\mu(\mathbf{x}) \geq 0$ for absorbing media.

The optical system in Fig. 1 consists of three parts: two ideal waveguides and a region with scattering and absorption. The coordinates in Fig. 1 are ones transformed using $\mathbf{x} = (x, y, z) \rightarrow (u, v, w)$, and they are used to apply a non-uniform mesh to Eqs. (1). Note that the Jacobian matrix of this transformation is diagonal in order to simplify the discussion in the following subsections **A-F**.

A. Discrete representation

Let us discretize the transformed space: $(u, v, w) \rightarrow (l, m, n)$, and let us use cells in Yee's lattice [18]. Figure 2 shows an arrangement of discretized functions (ϵ , μ , \mathbf{E} and \mathbf{H}) that are allocated a cell address (l, m, n) .

*Electronic address: t-usuki@petra-jp.org;
URL: <http://www.petra-jp.org/>

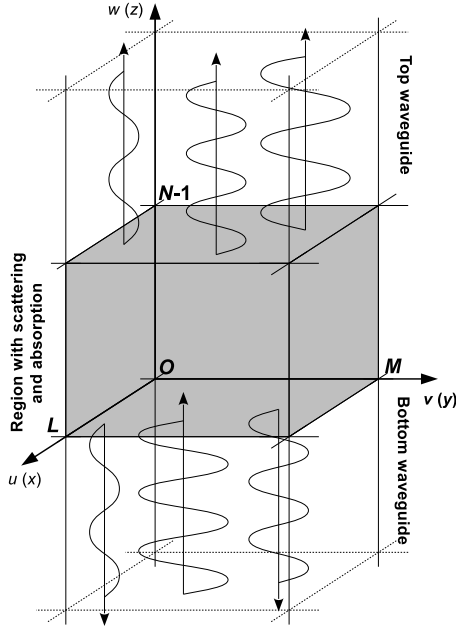


Figure 1: Optical system for multi-mode scattering. The propagation region is divided into three parts.

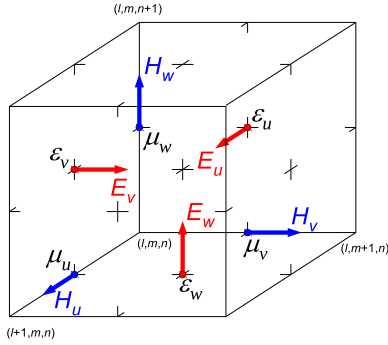


Figure 2: A (l, m, n) cell in Yee's lattice.

For example, the u component of the magnetic field $H_u(l, m, n)$ means H_u at $u = l + 1/2$, $v = m$, $w = n$ in the figure. The electromagnetic field in (x, y, z) coordinates is related to that of the (u, v, w) coordinates in the following manner.

$$\begin{aligned}\sqrt{\mu_0}H_x &= f_1(l) g_0(m) h_0(n) H_u(l, m, n), \\ \sqrt{\mu_0}H_y &= f_0(l) g_1(m) h_0(n) H_v(l, m, n), \\ \sqrt{\mu_0}H_z &= f_0(l) g_0(m) h_1(n) H_w(l, m, n),\end{aligned}\quad (2)$$

and

$$\begin{aligned}\sqrt{\varepsilon_0}E_x &= f_0(l) g_1(m) h_1(n) E_u(l, m, n), \\ \sqrt{\varepsilon_0}E_y &= f_1(l) g_0(m) h_1(n) E_v(l, m, n), \\ \sqrt{\varepsilon_0}E_z &= f_1(l) g_1(m) h_0(n) E_w(l, m, n),\end{aligned}\quad (3)$$

where f_k , g_k , and h_k are defined as

$$\begin{aligned}f_k^{-2}(l) &= \frac{\omega}{c} \frac{dx}{du} \Big|_{u=l+k/2}, \\ g_k^{-2}(m) &= \frac{\omega}{c} \frac{dy}{dv} \Big|_{v=m+k/2}, \\ h_k^{-2}(n) &= \frac{\omega}{c} \frac{dz}{dw} \Big|_{w=n+k/2}.\end{aligned}\quad (4)$$

Here, $c = 1/\sqrt{\varepsilon_0\mu_0}$ is the velocity of light in a vacuum. We make the domain of variables u and v finite: $0 \leq u < L$ and $0 \leq v < M$, where the boundaries L and M are integers. Furthermore, ε_η and μ_η for $\eta = u, v, w$ in Fig. 2 are defined as

$$\begin{aligned}\varepsilon_u(l, m, n) &= \varepsilon|_{u=l, v=m+1/2, w=n+1/2}, \\ \varepsilon_v(l, m, n) &= \varepsilon|_{u=l+1/2, v=m, w=n+1/2}, \\ \varepsilon_w(l, m, n) &= \varepsilon|_{u=l+1/2, v=m+1/2, w=n},\end{aligned}$$

and

$$\begin{aligned}\mu_u(l, m, n) &= \mu|_{u=l+1/2, v=m, w=n}, \\ \mu_v(l, m, n) &= \mu|_{u=l, v=m+1/2, w=n}, \\ \mu_w(l, m, n) &= \mu|_{u=l, v=m, w=n+1/2}.\end{aligned}$$

The relative permittivity ε_η and relative permeability μ_η for $\eta = u, v, w$ satisfy periodic conditions, i.e., $\varepsilon_\eta(l+L, m, n) = \varepsilon_\eta(l, m, n)$ and $\varepsilon_\eta(l, m+M, n) = \varepsilon_\eta(l, m, n)$. Figure 3 shows the coordinate transformation $(x, y) \rightarrow (u, v)$ described by Eqs. (A3) in Appendix A.

The six components of the electromagnetic field satisfy the following conditions:

$$\begin{aligned}\mathcal{G}(l+L, m, n) &= B_u \mathcal{G}(l, m, n), \\ \mathcal{G}(l, m+M, n) &= B_v \mathcal{G}(l, m, n),\end{aligned}$$

where $\mathcal{G} = H_\eta, E_\eta$ for $\eta = u, v, w$. The parameters B_u, B_v are generally complex numbers, and they satisfy $|B_u| = |B_v| = 1$. In this paper, $B_u = B_v = 1$. Now let us introduce the forward difference operators,

$$\begin{aligned}\Delta_u \mathcal{G}(l, m, n) &\triangleq \mathcal{G}(l+1, m, n) - \mathcal{G}(l, m, n), \\ \Delta_v \mathcal{G}(l, m, n) &\triangleq \mathcal{G}(l, m+1, n) - \mathcal{G}(l, m, n), \\ \Delta_w \mathcal{G}(l, m, n) &\triangleq \mathcal{G}(l, m, n+1) - \mathcal{G}(l, m, n).\end{aligned}\quad (5)$$

At $u = L-1$ and $v = M-1$, Δ_u and Δ_v are defined as

$$\begin{aligned}\Delta_u \mathcal{G}(L-1, m, n) &\triangleq B_u \mathcal{G}(0, m, n) - \mathcal{G}(L-1, m, n), \\ \Delta_v \mathcal{G}(l, M-1, n) &\triangleq B_v \mathcal{G}(l, 0, n) - \mathcal{G}(l, M-1, n).\end{aligned}$$

The backward difference operator is $-\Delta_u^T$, where “T” denotes the transpose. Using Eqs. (4) and (5), we can define modified difference operators:

$$\tilde{\Delta}_u = f_1 \Delta_u f_0, \quad \tilde{\Delta}_v = g_1 \Delta_v g_0, \quad \tilde{\Delta}_w = h_1 \Delta_w h_0. \quad (6)$$

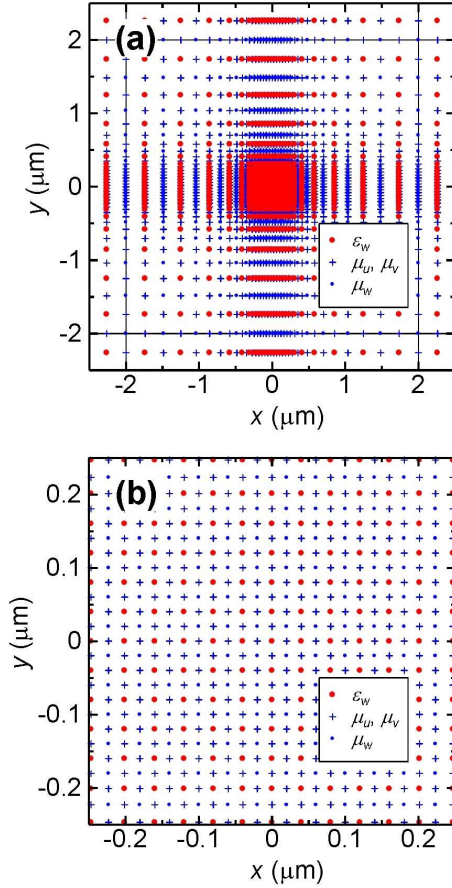


Figure 3: Grid of Yee's lattice in periodic xy space: $x(L) - x(0) = y(M) - y(0) = 4\mu\text{m}$ when $L = M = 25$, $\min(dx/du) = \min(dy/dv) = 40\text{ nm}$, and $K_u = K_v = 5$ (see Eq. (A3) in Appendix A). (a) Grid with periodic boundary conditions (dot-broken lines). (b) Grid around the origin.

From Eqs. (1) and (6), the u and v components of the electromagnetic field satisfy

$$\begin{aligned} \tilde{\Delta}_w \mathbf{H}_{uv}(n) &= i\mathbf{M}_{HE}(n) \mathbf{E}_{vu}(n), \\ -\tilde{\Delta}_w^T \mathbf{E}_{vu}(n) &= i\mathbf{M}_{EH}(n) \mathbf{H}_{uv}(n), \end{aligned} \quad (7)$$

with the $2LM \times 2LM$ matrices,

$$\begin{aligned} \mathbf{M}_{HE} &= \begin{pmatrix} -\tilde{\Delta}_u \boldsymbol{\mu}_w^{-1} \tilde{\Delta}_u^T + \boldsymbol{\varepsilon}_v & -\tilde{\Delta}_u \boldsymbol{\mu}_w^{-1} \tilde{\Delta}_v^T \\ -\tilde{\Delta}_v \boldsymbol{\mu}_w^{-1} \tilde{\Delta}_u^T & -\tilde{\Delta}_v \boldsymbol{\mu}_w^{-1} \tilde{\Delta}_v^T + \boldsymbol{\varepsilon}_u \end{pmatrix}, \\ \mathbf{M}_{EH} &= \begin{pmatrix} -\tilde{\Delta}_v^T \boldsymbol{\varepsilon}_w^{-1} \tilde{\Delta}_v + \boldsymbol{\mu}_u & \tilde{\Delta}_v^T \boldsymbol{\varepsilon}_w^{-1} \tilde{\Delta}_u \\ \tilde{\Delta}_u^T \boldsymbol{\varepsilon}_w^{-1} \tilde{\Delta}_v & -\tilde{\Delta}_u^T \boldsymbol{\varepsilon}_w^{-1} \tilde{\Delta}_u + \boldsymbol{\mu}_v \end{pmatrix}, \end{aligned} \quad (8)$$

and the $LM \times LM$ diagonal matrices,

$$\begin{aligned} \boldsymbol{\varepsilon}_\eta &= \text{diag}(\varepsilon_\eta(0, 0, n), \dots, \varepsilon_\eta(L-1, M-1, n)), \\ \boldsymbol{\mu}_\eta &= \text{diag}(\mu_\eta(0, 0, n), \dots, \mu_\eta(L-1, M-1, n)). \end{aligned}$$

The $2LM \times 1$ column vectors \mathbf{H}_{uv} and \mathbf{E}_{vu} in Eq. (7) are expressed as

$$\mathbf{H}_{uv} = \begin{pmatrix} \mathbf{H}_u \\ \mathbf{H}_v \end{pmatrix}, \quad \mathbf{E}_{vu} = \begin{pmatrix} -\mathbf{E}_v \\ \mathbf{E}_u \end{pmatrix}.$$

Here,

$$\begin{aligned} \mathbf{H}_\eta &= (H_\eta(0, 0, n) \cdots H_\eta(L-1, M-1, n))^T, \\ \mathbf{E}_\eta &= (E_\eta(0, 0, n) \cdots E_\eta(L-1, M-1, n))^T. \end{aligned}$$

From Eqs. (1), the w -components H_w in Eqs.(2) and E_w in Eqs.(3) can be expressed as

$$\begin{aligned} \mathbf{E}_w(n) &= \frac{i}{\boldsymbol{\varepsilon}_w(n)} \left(\tilde{\Delta}_u \mathbf{H}_v(n) - \tilde{\Delta}_v \mathbf{H}_u(n) \right), \\ \mathbf{H}_w(n) &= \frac{i}{\boldsymbol{\mu}_w(n)} \left(\tilde{\Delta}_u^T \mathbf{E}_v(n) - \tilde{\Delta}_v^T \mathbf{E}_u(n) \right). \end{aligned}$$

B. Wave propagation in ideal waveguides

For the bottom ideal waveguide, \mathbf{M}_{HE} , \mathbf{M}_{EH} of Eqs. (8) and h_j in Eqs. (4) are

$$\begin{aligned} \mathbf{M}_{HE}(n) &= \mathbf{M}_{bHE}, \quad \mathbf{M}_{EH}(n) = \mathbf{M}_{bEH}, \\ h_0(n) &= h_1(n) = h_b, \text{ as } n \leq 0. \end{aligned}$$

For the top ideal waveguide, they are

$$\begin{aligned} \mathbf{M}_{HE}(n) &= \mathbf{M}_{tHE}, \quad \mathbf{M}_{EH}(n) = \mathbf{M}_{tEH}, \\ h_0(n) &= h_1(n) = h_t, \text{ as } n \geq N-1. \end{aligned}$$

Since the permittivity in the ideal waveguides is real, we have

$$\text{Im} \mathbf{M}_{\kappa HE} = \text{Im} \mathbf{M}_{\kappa EH} = 0 \quad (9)$$

for $\kappa = b, t$. Figure 4 depicts the arrangement of the above equations. The eigenvalue equation for the optical

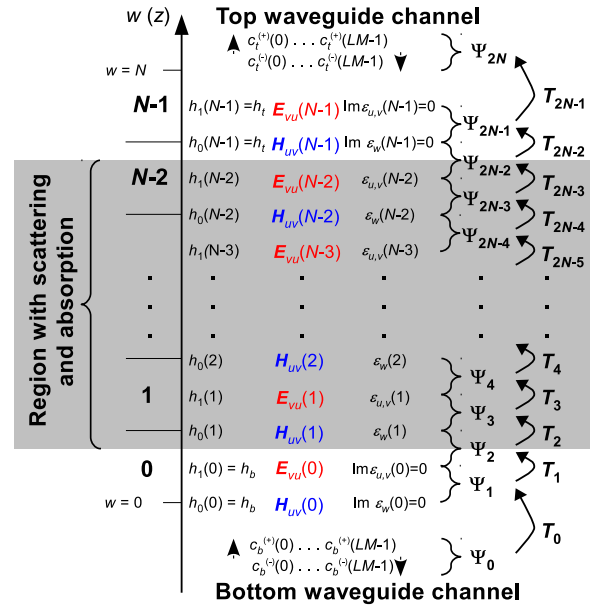


Figure 4: Graphic depiction of Eqs. (9)-(19).

modes of the ideal waveguides is

$$\mathbf{M}_{\kappa HE} \mathbf{M}_{\kappa EH} \mathbf{u}_{\kappa}(j) = \Lambda_{\kappa}^2(j) \mathbf{u}_{\kappa}(j), \quad (10)$$

for $0 \leq j < LM$. Here, \mathbf{u}_{κ} are eigenvectors. Appendix B show that all eigenvectors satisfy

$$\mathbf{u}_{\kappa}^T(j) \mathbf{M}_{\kappa EH} \mathbf{u}_{\kappa}(j') - \delta_{jj'} = 0, \quad (11)$$

where $\delta_{jj'}$ is Kronecker's delta. The propagation constants β_b and β_t are given by

$$\beta_{\kappa}(j) = 2 \arcsin \frac{\Lambda_{\kappa}(j)}{2h_{\kappa}^2} \text{ for } \kappa = b, t, \quad (12)$$

and $0 \leq \arg \beta_{\kappa}(j) < \pi$. We use an integer J_{κ} to separate the propagating modes and evanescent modes of the above β_{κ} : $\text{Im} \beta_{\kappa}(j) = 0$ as $0 \leq j < J_{\kappa}$, and $\text{Im} \beta_{\kappa}(j) \neq 0$ as $J_{\kappa} \leq j < LM$. We build a square matrix consisting of the eigenmodes \mathbf{u}_{κ} of Eq. (10), a diagonal matrix $\boldsymbol{\theta}_{\kappa}$ from Eq. (12) consisting of the phases of the modes, and column vectors $\boldsymbol{\psi}_{\kappa}^{(\pm)}$ consisting of the coefficients $c_{\kappa}^{(\pm)}(j)$ of the j -th mode in the waveguides:

$$\begin{aligned} \mathbf{U}_{\kappa} &= (\mathbf{u}_{\kappa}(0) \cdots \mathbf{u}_{\kappa}(LM-1)), \\ \boldsymbol{\theta}_{\kappa} &= \text{diag}(\exp(i\beta_{\kappa}(0)), \dots, \exp(i\beta_{\kappa}(LM-1))), \\ \boldsymbol{\psi}_{\kappa}^{(\pm)} &= (c_{\kappa}^{(\pm)}(0) \cdots c_{\kappa}^{(\pm)}(LM-1))^T. \end{aligned} \quad (13)$$

Note that $\mathbf{U}_{\kappa}^T \mathbf{M}_{\kappa EH} \mathbf{U}_{\kappa} = \mathbf{1}$ from Eq. (11). The $\mathbf{H}_{uv}(0)$ and $\mathbf{E}_{vu}(0)$ in the bottom ideal waveguide are defined by using Eq. (13):

$$\begin{aligned} \mathbf{H}_{uv}(0) &= \mathbf{U}_b (\boldsymbol{\psi}_b^{(+)} + \boldsymbol{\psi}_b^{(-)}), \\ \mathbf{E}_{vu}(0) &= \frac{i}{h_b^2} \mathbf{M}_{bEH} \mathbf{U}_b \\ &\quad \times \left(\frac{1}{1 - \boldsymbol{\theta}_b^{-1}} \boldsymbol{\psi}_b^{(+)} + \frac{1}{1 - \boldsymbol{\theta}_b} \boldsymbol{\psi}_b^{(-)} \right). \end{aligned} \quad (14)$$

The $\mathbf{H}_{uv}(N-1)$ and $\mathbf{E}_{vu}(N-1)$ in the top ideal waveguide are defined in the same manner.

C. Power flow with absorption

Let us define the discretized formulation of time averaged power flow [19]:

$$P_z(n) \triangleq \frac{c^3}{2\omega^2} \text{Re} \left(\mathbf{E}_{vu}^{\dagger}(n) h_1(n) h_0(n) \mathbf{H}_{uv}(n) \right), \quad (15)$$

where “ \dagger ” denotes the Hermitian conjugate. From Eqs. (12), (13) and (14), the power flows $P_{bz} = P_z(0)$ and $P_{tz} = P_z(N-1)$ for Eq. (15) are given by

$$\begin{aligned} P_{\kappa z} &= \sum_{j=0}^{J_{\kappa}-1} \gamma_{\kappa}^2(j) \left(\left| c_{\kappa}^{(+)}(j) \right|^2 - \left| c_{\kappa}^{(-)}(j) \right|^2 \right), \\ \gamma_{\kappa}(j) &= \sqrt{\frac{c^3}{4\omega^2} \cot \left(\frac{\beta_{\kappa}(j)}{2} \right)}, \end{aligned} \quad (16)$$

where γ_{κ} is real and positive. Equations (7), (15), and (16) lead to the following relation between power flow and absorption:

$$\begin{aligned} P_{bz} - P_{tz} &= \frac{c^3}{2\omega^2} \sum_{n=1}^{N-2} \left[\mathbf{E}_{vu}^{\dagger}(n) (\text{Im} \mathbf{M}_{HE}(n)) \mathbf{E}_{vu}(n) \right. \\ &\quad \left. + \mathbf{H}_{uv}^{\dagger}(n) (\text{Im} \mathbf{M}_{EH}(n)) \mathbf{H}_{uv}(n) \right] \\ &= \frac{c^3}{2\omega^2} \sum_{n=1}^{N-2} \sum_{\eta=u,v,w} \left[\mathbf{E}_{\eta}^{\dagger}(n) (\text{Im} \boldsymbol{\epsilon}_{\eta}(n)) \mathbf{E}_{\eta}(n) \right. \\ &\quad \left. + \mathbf{H}_{\eta}^{\dagger}(n) (\text{Im} \boldsymbol{\mu}_{\eta}(n)) \mathbf{H}_{\eta}(n) \right]. \end{aligned} \quad (17)$$

D. Transfer matrices

We make $4LM \times 1$ column vectors $\boldsymbol{\Psi}_k$ of the electromagnetic modes and $4LM \times 4LM$ matrices \mathbf{T}_k , which we call transfer matrices: $\boldsymbol{\Psi}_{k+1} = \mathbf{T}_k \boldsymbol{\Psi}_k$. The $\boldsymbol{\Psi}_k$ are defined as

$$\begin{aligned} \boldsymbol{\Psi}_0 &= \begin{pmatrix} \boldsymbol{\psi}_b^{(+)} \\ \boldsymbol{\psi}_b^{(-)} \end{pmatrix}, \quad \boldsymbol{\Psi}_{2N} = \begin{pmatrix} \boldsymbol{\psi}_t^{(+)} \\ \boldsymbol{\psi}_t^{(-)} \end{pmatrix}, \\ \boldsymbol{\Psi}_{2n-1} &= \begin{pmatrix} \mathbf{H}_{uv}(n-1) \\ \mathbf{E}_{vu}(n-1) \end{pmatrix} \quad \text{for } 1 \leq n \leq N, \\ \boldsymbol{\Psi}_{2n} &= \begin{pmatrix} \mathbf{E}_{vu}(n-1) \\ \mathbf{H}_{uv}(n) \end{pmatrix} \quad \text{for } 1 \leq n \leq N-1. \end{aligned}$$

Equations (7) and (14) yield the transfer matrices:

$$\begin{aligned} \mathbf{T}_0 &= \begin{pmatrix} \mathbf{U}_b & \mathbf{U}_b \\ \frac{i\mathbf{M}_{bEH}\mathbf{U}_b}{h_b^2} \frac{1}{1-\boldsymbol{\theta}_b^{-1}} & \frac{i\mathbf{M}_{bEH}\mathbf{U}_b}{h_b^2} \frac{1}{1-\boldsymbol{\theta}_b} \end{pmatrix}, \\ \mathbf{T}_{2n-1} &= \begin{pmatrix} \mathbf{0} & \mathbf{1} \\ \frac{h_0(n-1)}{h_0(n)} & \frac{i\mathbf{M}_{HE}(n-1)}{h_0(n)h_1(n-1)} \end{pmatrix}, \\ \mathbf{T}_{2n} &= \begin{pmatrix} \mathbf{0} & \mathbf{1} \\ \frac{h_1(n-1)}{h_1(n)} & \frac{i\mathbf{M}_{EH}(n)}{h_1(n)h_0(n)} \end{pmatrix}, \quad 1 \leq n \leq N-1. \end{aligned} \quad (18)$$

For \mathbf{T}_{2N-1} , we have

$$\mathbf{T}_{2N-1} = \begin{pmatrix} \mathbf{0} & -ih_t^2(1-\boldsymbol{\theta}_t^{-1})\mathbf{U}_t^T \\ \mathbf{1} & ih_t^2\mathbf{U}_t(1-\boldsymbol{\theta}_t^{-1})\mathbf{U}_t^T \end{pmatrix}. \quad (19)$$

By using Eqs. (18) and (19), we can obtain the $2LM \times 2LM$ matrices $\hat{\mathbf{t}}$ and $\hat{\mathbf{r}}$ from the linear equation:

$$\begin{pmatrix} \hat{\mathbf{t}} \\ \mathbf{0} \end{pmatrix} = \mathbf{T}_{2N-1} \cdots \mathbf{T}_0 \begin{pmatrix} \mathbf{1} \\ \hat{\mathbf{r}} \end{pmatrix}, \quad (20)$$

which is the same as Eq. (2.17) in our previous study [16].

E. Stable transfer matrix method

To solve the above Eq. (20), we can establish a stable iterative procedure [16, 17] by using the $4LM \times 4LM$ column operator \mathbf{P}_j . This procedure does not entail solving multi-slice eigenvalue problems for the region with scattering and absorption, which has advantages in both computational time and numerical precision over the other procedure [20, 21] that can be applied to optical scattering [12–15]. In the following discussion, suppose we have $2LM \times 2LM$ blocks of matrices \mathcal{M} and \mathcal{N} notated by

$$\mathcal{M} = \begin{pmatrix} \mathcal{M}_{00} & \mathcal{M}_{01} \\ \mathcal{M}_{10} & \mathcal{M}_{11} \end{pmatrix} \quad \text{and} \quad \mathcal{N} = \begin{pmatrix} \mathcal{N}_{00} & \mathcal{N}_{01} \end{pmatrix}.$$

The iterative equations for the $4LM \times 4LM$ matrix \mathbf{C}_k and the $2LM \times 4LM$ matrix \mathbf{D}_k can be used to find $\hat{\mathbf{t}}$ and $\hat{\mathbf{r}}$:

$$\begin{aligned} \mathbf{C}_{k+1} &= \mathbf{T}_k \mathbf{C}_k \mathbf{P}_k, \\ \mathbf{D}_{k+1} &= \mathbf{D}_k \mathbf{P}_k \quad \text{for } 0 \leq k \leq 2N-1. \end{aligned} \quad (21)$$

The initial conditions are that

$$\mathbf{C}_0 = \begin{pmatrix} \mathbf{1} & \mathbf{0} \\ \mathbf{0} & \mathbf{1} \end{pmatrix} \quad \text{and} \quad \mathbf{D}_0 = \begin{pmatrix} \mathbf{0} & \mathbf{1} \end{pmatrix}. \quad (22)$$

\mathbf{C}_k always satisfies

$$\mathbf{C}_k = \begin{pmatrix} \mathbf{C}_{k,00} & \mathbf{C}_{k,01} \\ \mathbf{0} & \mathbf{1} \end{pmatrix}$$

because of the column operator \mathbf{P}_k in Eq. (21). \mathbf{P}_k has the following matrix representation:

$$\mathbf{P}_k = \begin{pmatrix} \mathbf{1} \\ -\frac{\mathbf{1}}{\mathbf{T}_{k,10}\mathbf{C}_{k,01}+\mathbf{T}_{k,11}}\mathbf{T}_{k,10}\mathbf{C}_{k,00} \\ \mathbf{0} \\ \frac{\mathbf{1}}{\mathbf{T}_{k,10}\mathbf{C}_{k,01}+\mathbf{T}_{k,11}} \end{pmatrix}, \quad (23)$$

and here, the actual numerical procedure uses Gaussian elimination *without* partial pivoting for \mathbf{P}_{k11} . From Eqs. (22) and (23), we find that iterating Eq. (21) gives us

$$\hat{\mathbf{t}} = \mathbf{C}_{2N,00} \quad \text{and} \quad \hat{\mathbf{r}} = \mathbf{D}_{2N,00}.$$

We can compute the electromagnetic field in the scattering region by making $2LM \times 4LM$ matrices $\hat{\mathcal{E}}(n, k)$ for \mathbf{E}_{vu} and $\hat{\mathcal{H}}(n, k)$ for \mathbf{H}_{uv} for the n -th cell. The initial conditions are

$$\hat{\mathcal{E}}(n, 2n+1) = \hat{\mathcal{H}}(n, 2n) = \begin{pmatrix} \mathbf{0} & \mathbf{1} \end{pmatrix}$$

for $1 \leq n \leq N-2$. The $\hat{\mathcal{E}}(n, k)$ and $\hat{\mathcal{H}}(n, k)$ are iterated using the column operator \mathbf{P}_k :

$$\begin{aligned} \hat{\mathcal{E}}(n, k+1) &= \hat{\mathcal{E}}(n, k) \mathbf{P}_k \quad \text{for } 2n+1 \leq k \leq 2N-1, \\ \hat{\mathcal{H}}(n, k+1) &= \hat{\mathcal{H}}(n, k) \mathbf{P}_k \quad \text{for } 2n \leq k \leq 2N-1. \end{aligned}$$

Appendices C and D give two approaches to simulating the reverse scattering process from the top ideal waveguide to the bottom ideal waveguide. We can use either of these approaches to obtain $\hat{\mathbf{t}}'$, $\hat{\mathbf{r}}'$, $\hat{\mathcal{E}}'(n, k)$ and $\hat{\mathcal{H}}'(n, k)$ for the reverse process.

F. Scattering matrix

Let us define a $J_b \times J_b$ matrix \mathbf{r} and a $J_t \times J_b$ matrix \mathbf{t} only for propagating wave modes. The elements of \mathbf{r} and \mathbf{t} are normalized to $\hat{\mathbf{r}}$ and $\hat{\mathbf{t}}$ by the power flow of Eq. (16) as follows:

$$r_{jj'} = \frac{\gamma_b(j)}{\gamma_b(j')} \hat{r}_{jj'}, \quad t_{jj'} = \frac{\gamma_t(j)}{\gamma_b(j')} \hat{t}_{jj'}.$$

If we only obtain the matrices \mathbf{r} and \mathbf{t} , we can reduce the matrix sizes of \mathbf{C}_k and \mathbf{D}_k : $2LM \times J_b$ blocks $\mathbf{C}_{k,00}$ and $\mathbf{C}_{k,10}$, $2LM \times 2LM$ blocks $\mathbf{C}_{k,01}$ and $\mathbf{C}_{k,11}$, a $J_b \times J_b$ block $\mathbf{D}_{k,10}$, and a $J_b \times 2LM$ block $\mathbf{D}_{k,11}$. By using the matrices $\hat{\mathbf{r}}'$ and $\hat{\mathbf{t}}'$, we can define a $J_t \times J_t$ matrix \mathbf{r}' and a $J_b \times J_t$ matrix \mathbf{t}' . In so doing, we obtain a $(J_b + J_t) \times (J_b + J_t)$ S-matrix [11]:

$$\mathbf{S} = \begin{pmatrix} \mathbf{r} & \mathbf{t}' \\ \mathbf{t} & \mathbf{r}' \end{pmatrix}. \quad (24)$$

Let us define $2LM \times J_b$ matrices $\mathcal{E}(n)$, $\mathcal{H}(n)$

$$\begin{aligned} (\mathcal{E}(n))_{jj'} &= \frac{(\hat{\mathcal{E}}_{00}(n, 2N))_{jj'}}{\gamma_b(j')}, \\ (\mathcal{H}(n))_{jj'} &= \frac{(\hat{\mathcal{H}}_{00}(n, 2N))_{jj'}}{\gamma_b(j')}. \end{aligned}$$

and $2LM \times J_t$ matrices \mathcal{E}' , \mathcal{H}' only for propagating wave modes. We also define a $4LM \times (J_b + J_t)$ matrix $\boldsymbol{\xi}_n$ and a $4LM \times 4LM$ matrix $\boldsymbol{\alpha}_n$

$$\begin{aligned} \boldsymbol{\xi}_n &= \begin{pmatrix} \mathcal{E}(n) & \mathcal{E}'(n) \\ \mathcal{H}(n) & \mathcal{H}'(n) \end{pmatrix}, \\ \boldsymbol{\alpha}_n &= \frac{c^3}{2\omega^2} \begin{pmatrix} \text{Im}\mathbf{M}_{HE}(n) & \mathbf{0} \\ \mathbf{0} & \text{Im}\mathbf{M}_{EH}(n) \end{pmatrix}. \end{aligned} \quad (25)$$

From Eqs. (17) and (25), the S-matrix including the case of absorption media satisfies

$$\mathbf{S}^\dagger \mathbf{S} - \mathbf{1} + \sum_{n=1}^{N-2} \boldsymbol{\xi}_n^\dagger \boldsymbol{\alpha}_n \boldsymbol{\xi}_n = \mathbf{0}. \quad (26)$$

This equation shows that the S-matrix is unitary when $\text{Im}\mathbf{M}_{HE}(n) = \text{Im}\mathbf{M}_{EH}(n) = 0$ for $0 \leq n \leq N-1$.

III. NUMERICAL RESULTS

The method described in the previous section is suitable for analyzing very small scattering coefficients. Here, we will discuss the optical properties of a sidewall grating waveguide (SGW) that is part of a phase shifter in a silicon optical modulator [22]. The grating structure is used to inject free carriers into the waveguide core, but

for it to work properly, the reflections of the fundamental mode and radiation loss from the structure have to be suppressed.

Figure 5 shows the SGW and its permittivity [23] distribution. The SGW is a silicon waveguide and has a SiO_2 cladding layer on which a vacuum region is set. For the numerical analysis, we set the waveguide core to $440 \text{ nm} \times 220 \text{ nm}$ and the grating pitch (width) to $284 \text{ (} 74.5 \text{) nm}$. Before conducting the simulation, we have

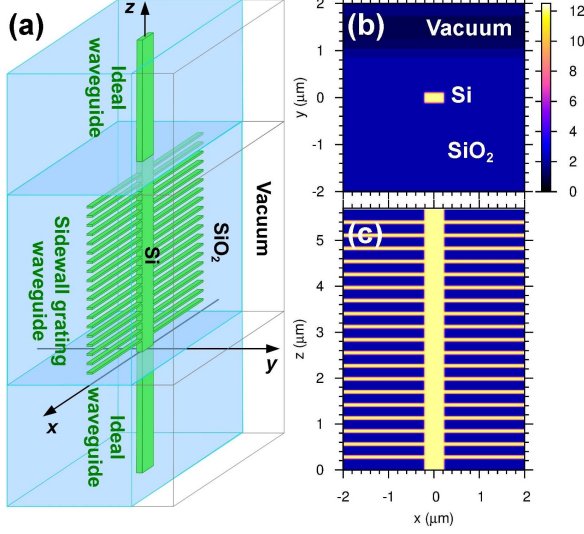


Figure 5: (a) SGW. (b) Permittivity distribution on xy -plane at $z = 0$. (c) Distribution on zx -plane at $y = 0$.

to obtain optical modes for the ideal waveguides at both ends of the SGW. The ideal waveguides have three waveguide modes and many radiation modes, as shown in Fig. 6. The propagating mode numbers J_b and J_t are that

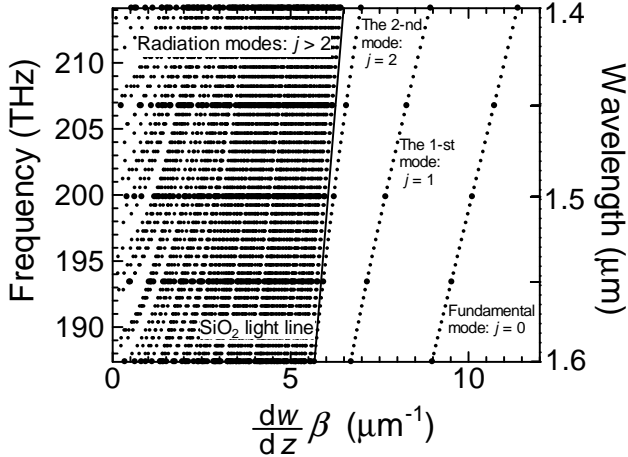


Figure 6: Dispersion diagram of Si waveguide. There are three waveguide modes and many radiation modes in the SiO_2 cladding layer and vacuum layer.

$J_b = J_t = 125 - 96$ at $1.4 - 1.6 \mu\text{m}$, because we set four μm periodic boundary conditions along the x and y axes.

The grid parameters of x and y are the same as in Fig. 3, whereas the grid parameters of z are $dz/dw = 28.4 \text{ nm}$ and $N = 200$. Figure 7 shows cross sections of the waveguide modes and radiation modes at a wavelength of $1.55 \mu\text{m}$. The three waveguide modes in Fig. 7(a)-(c) are la-

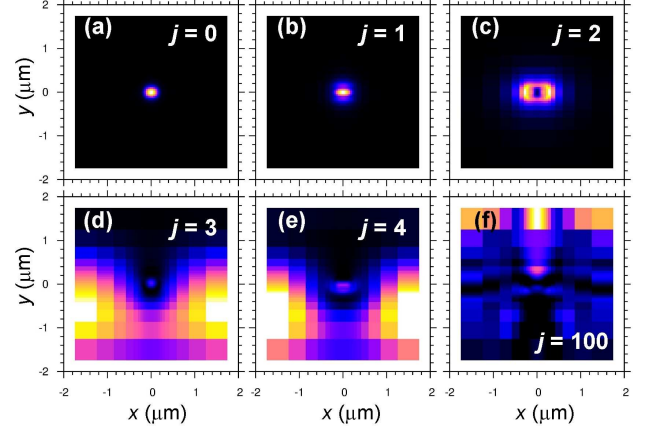


Figure 7: Optical modes for Si waveguide at $1.55 \mu\text{m}$. (a) $j = 0$: E_{11}^x . (b) $j = 1$: E_{11}^y . (c) $j = 2$: E_{21}^x . (d) $j = 3$: radiation mode in the SiO_2 cladding layer. (e) $j = 4$: radiation mode in the SiO_2 cladding layer. (f) $j = 100$: radiation mode in the vacuum layer.

beled E_{11}^x , E_{11}^y and E_{21}^x [19]. The waveguide modes are clearly localized around the silicon waveguide core. From the x -axis symmetry of the SGW, the fundamental mode E_{11}^x scattering through the SGW is intra-mode scattering (i.e. reflection) when the scattering only occurs between the waveguide modes. However, the scattering process between the E_{11}^x and radiation modes is complex. Figure 7(d)-(f) shows three of the 100 radiation modes. The optical power outside the core is dominant for each radiation mode, but remains small inside the core. Therefore, we have to consider not only the reflection within the E_{11}^x but also scattering between E_{11}^x and other modes including radiation modes.

Figure 8 shows the transmittance and reflectance of the SGW when E_{11}^x is launched from the bottom. There is a stop band at around $1.45 \mu\text{m}$, after which the fundamental-mode reflectance decreases with a periodic modification of increasing wavelength. The reflectance of each radiation mode also has a strong wavelength dependence. In particular, it has a low value at the point of the third mode reflectance in Fig. 8. The total optical loss, which is caused by E_{11}^x reflection and radiation-mode scattering, is 4.39% (-13.6 dB) at a wavelength of $1.55 \mu\text{m}$. Note that the loss does not have so strong a wavelength dependence. The simulation results clearly show that the sidewall grating does not cause significant losses or reflections for the silicon optical interposer [5].

In an actual phase shifter [22], the gratings on either side of the waveguide core are doped with donors or acceptors, and aluminum electrodes are attached to the gratings (see Fig. 9). Doped silicon [25, 26] with metal

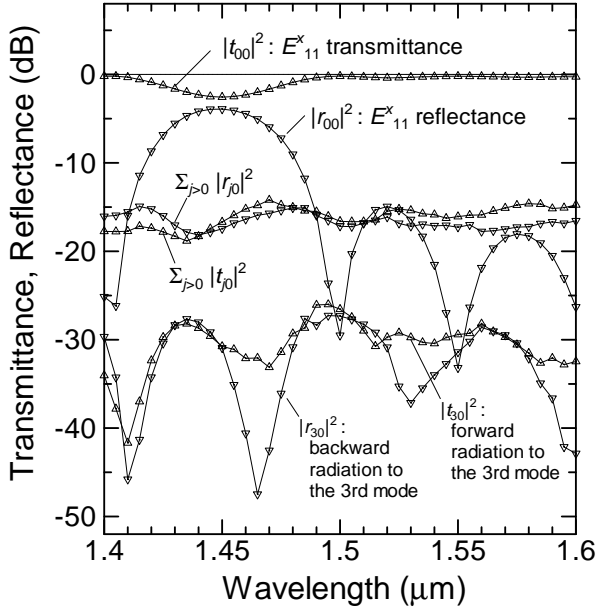


Figure 8: Optical scattering from the fundamental mode. The SGW has a stop band at $1.45 \mu\text{m}$. This is a typical filtering property for $|r_{00}|^2$, and it is designed for a modulator with low optical loss in the range of $1531 - 1591 \text{ nm}$ [24]. The radiation and reflection loss is about -15 dB respectively.

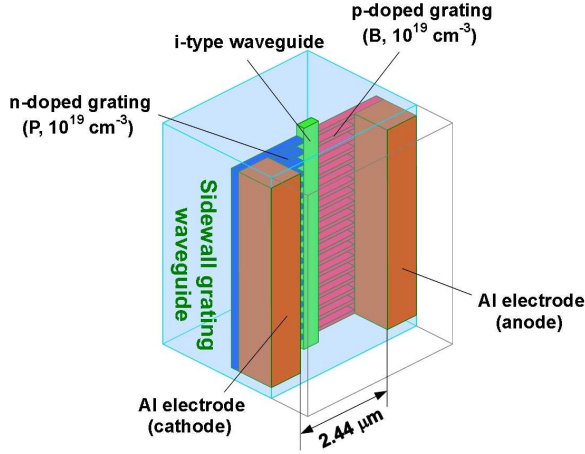


Figure 9: P-i-n diode in SGW. The left (right) side of the side wall grating is doped with a donor (acceptor) density 10^{19} cm^{-3} . The electrodes' gap is $2.44 \mu\text{m}$. The permittivity of doped silicon is taken from [25, 26], and the permittivity of aluminum is taken from [27, 28].

electrodes [27, 28] changes the optical index and absorption properties of the SGW. We calculated the scattering process for absorption at a wavelength of $1.55 \mu\text{m}$. Figure 10 shows the distribution of $|t_{j0}|^2$ and $|r_{j0}|^2$ as $0 \leq j < 103$. The total optical loss is 5.59% (-12.5 dB), and it consists of E_{11}^x reflection (see the case of $j = 0$ in Fig. 10), E_{21}^x scattering ($j = 2$), radiation-mode scattering ($3 \leq j < 103$), and absorption loss (0.52% (-22.8 dB)). Note that the distribution around -80 dB

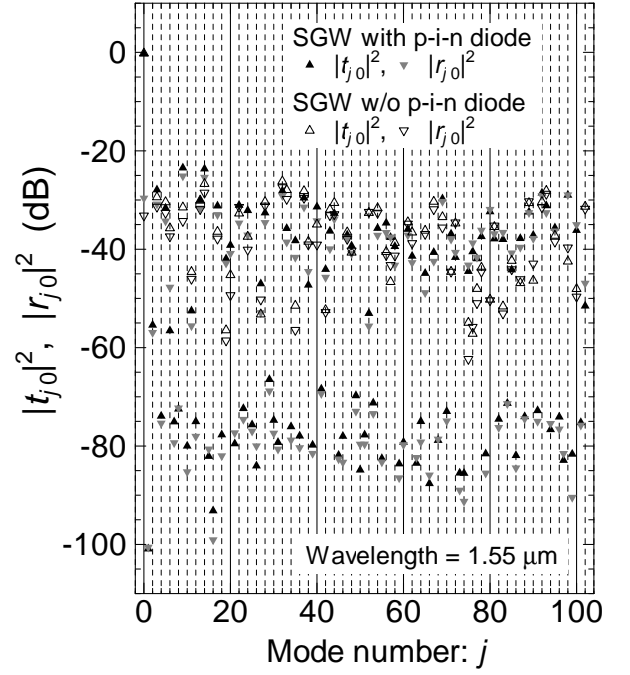


Figure 10: Distribution of scattering coefficients on the SGW at $1.55 \mu\text{m}$. The distribution at around -30 dB of the SGW with the p-i-n diode is not so different from that of the SGW without the diode.

and the E_{21}^x scattering are caused by an x -axis asymmetry due to the different optical indexes of the p-doped and n-doped regions [25, 26].

IV. CONCLUSIONS

This proposed method can calculate scattering coefficients for all incident modes from the bottom waveguide and the top waveguide. To determine the precision numerically, we use the max norm S_{\max} on the left side of Eq. (26):

$$S_{\max} = \left\| \mathbf{S}^\dagger \mathbf{S} - \mathbf{1} + \sum_{n=1}^{N-2} \boldsymbol{\xi}_n^\dagger \boldsymbol{\alpha}_n \boldsymbol{\xi}_n \right\|_{\max} \quad (27)$$

and the max norm $U_{\kappa \max}$ on the left side of Eq. (11) for the propagation modes:

$$U_{\kappa \max} = \left\| (\mathbf{u}_\kappa(0) \cdots \mathbf{u}_\kappa(J_\kappa - 1))^\dagger \mathbf{M}_{\kappa EH} \right. \\ \left. \times (\mathbf{u}_\kappa(0) \cdots \mathbf{u}_\kappa(J_\kappa - 1)) - \mathbf{1} \right\|_{\max}. \quad (28)$$

We can estimate the numerical error of the obtained scattering coefficients by performing a double precision calculation of Eqs. (27) and (28). Figure 11 shows that numerical error of the eigenvalue calculation for ideal waveguide modes causes S_{\max} error. Using the Type I reverse propagation described in Appendix C results in an S_{\max} value of less than 10^{-8} . On the other hand, the

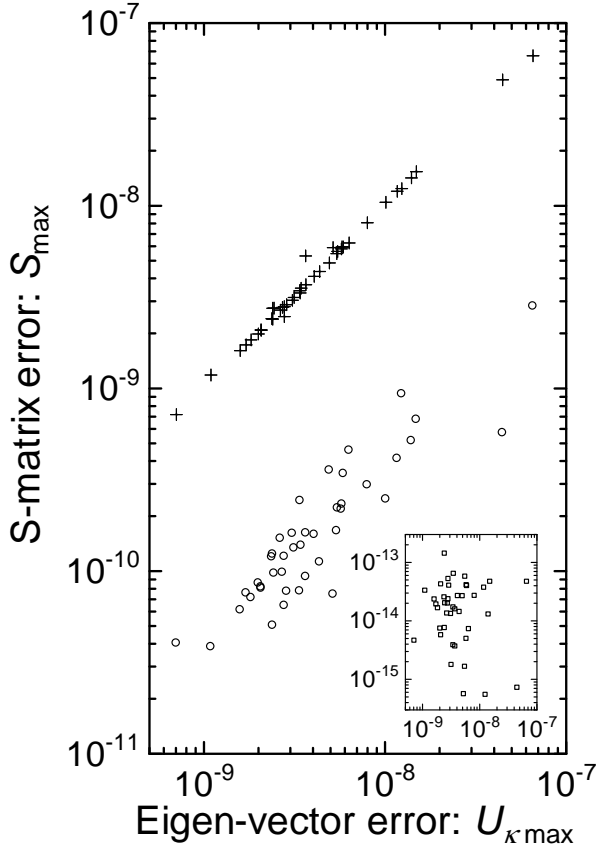


Figure 11: $U_{k \max}$ dependence of S_{\max} . Circles (crosses) indicate Type I (II) results. $U_{b \max} = U_{t \max}$ in this case. The inset plots the absolute value of the 00-element on the left side of Eq. (11).

numerical error of the power-flow conservation for E_{11}^x scattering does not depend on $U_{k \max}$, and it is less than 2×10^{-13} , as shown in the inset of Fig. 11. Therefore, our method satisfies the condition placed on the S-matrix (Eq. (27)) and gives us detailed optical properties with high enough precision for designing silicon photonics devices [5, 22]. For typical simulations, we recommend the Type II in Appendix D, because it takes only about half of the computational effort of Type I.

We will use this method to analyze low and complex optical scattering cases. Furthermore, the discretization of the permittivity distribution on the Yee lattice is compatible with FDTD. By combining this method and FDTD, numerical analyses with an optical propagation model can be made general and detailed.

Acknowledgments

The author would like to thank Makoto Okano for telling me about the FDTD method, Suguru Akiyama and Takeshi Baba for their fruitful discussions on Sec. III of this paper, and Motomu Takatsu for his helpful comments on Appendix B. This work was supported by the

“Funding Program for World-Leading Innovative R&D on Science and Technology (FIRST Program).”

Appendix A: Non-uniform mesh for equations (4)

Here, we show the details of the coordinate transformation. The periodic boundary conditions should be applied to dx/du and dy/dv :

$$\frac{dx}{du}(u) = \frac{dx}{du}(u + L), \quad \frac{dy}{dv}(v) = \frac{dy}{dv}(v + M).$$

We introduce the periodic function $F(\xi, K)$ into dx/du and dy/dv .

$$F(\xi, K) = 2^{2K-1} \cos^{2K}(\pi\xi) \prod_{J=1}^{K-1} \frac{J}{K+J}. \quad (\text{A1})$$

The function (A1) has several properties:

$$\begin{aligned} F(\xi + 1, K) &= F(-\xi, K) = F(\xi, K), \\ \max F(\xi, K) &= F(0, K) = 2^{2K-1} \prod_{J=1}^{K-1} \frac{J}{K+J}, \\ \min F(\xi, K) &= F\left(\frac{1}{2}, K\right) = 0, \end{aligned}$$

$$\int_0^1 F(\xi, K) d\xi = 1,$$

$$\lim_{K \rightarrow \infty} F(\xi, K) = \sum_{I=-\infty}^{\infty} \delta(\xi - I),$$

where $\delta(\xi)$ is the Dirac delta function. From Eq. (A1), we obtain an analytical formula for the integral of $F(\xi, K)$.

$$\begin{aligned} &\int_0^\xi F(\xi', K) d\xi' \\ &= \xi + \sum_{J=1}^K 2 \left(\prod_{J'=1}^J \frac{K - J + J'}{K + J'} \right) \frac{\sin(2\pi J\xi)}{2\pi J}. \end{aligned} \quad (\text{A2})$$

The integral of F has a staircase shape. For example, we can set $x(u)$ and $y(v)$ by using

$$\begin{aligned} \frac{x(u) - x(0) - u \min(dx/du)}{x(L) - x(0) - L \min(dx/du)} &= \int_0^{u/L} F(\xi, K_u) d\xi, \\ \frac{y(v) - y(0) - v \min(dy/dv)}{y(M) - y(0) - M \min(dy/dv)} &= \int_0^{v/M} F(\xi, K_v) d\xi, \end{aligned} \quad (\text{A3})$$

given ten parameters $L, M, x(0), y(0), x(L), y(M), \min(dx/du), \min(dy/dv), K_u$ and K_v .

Appendix B: Orthogonality of eigenvalue equation (10)

We should note that $\mathbf{u}_\kappa^\dagger(j) \mathbf{M}_{\kappa EH} \mathbf{u}_\kappa(j) = 0$, where “ \dagger ” denotes the Hermitian conjugate, when $\text{Im}\Lambda_\kappa^2(j) \neq 0$, and that no linear combination $a\mathbf{M}_{\kappa EH} + b\mathbf{M}_{\kappa HE}^{-1}$ (real a, b) is positive definite. However, the eigenvector \mathbf{u}_κ still satisfies

$$\mathbf{u}_\kappa^T(j) \mathbf{M}_{\kappa EH} \mathbf{u}_\kappa(j) \neq 0.$$

As an example, let us consider a simple equation, $\begin{pmatrix} 0 & 1 \\ 1 & 0 \end{pmatrix} \mathbf{u} = \lambda \begin{pmatrix} 1 & 0 \\ 0 & -1 \end{pmatrix} \mathbf{u}$, where the matrix $\begin{pmatrix} b & a \\ a & -b \end{pmatrix}$ is not positive definite. This equation has complex eigenvalues and eigenvectors: $\lambda_\pm = \pm i$, $\mathbf{u}_\pm = \begin{pmatrix} 1 \\ \pm i \end{pmatrix}$, and

$$\mathbf{u}_\pm^T \begin{pmatrix} 1 & 0 \\ 0 & -1 \end{pmatrix} \mathbf{u}_\pm \neq 0.$$

Therefore, we can normalize all eigenvectors as

$$\mathbf{u}_\kappa^T(j) \mathbf{M}_{\kappa EH} \mathbf{u}_\kappa(j') = \delta_{jj'}$$

when eigenvalues are non-zero and non-degenerate, and number of eigenvalues is equal to the order of $\mathbf{M}_{\kappa EH}$. The eigenvalue equations for the numerical results of Sec. III satisfy this condition.

We recommend checking which eigenvalue equations satisfy the condition or not, because there exists a counter example: $\begin{pmatrix} 2 & 1 \\ 1 & 0 \end{pmatrix} \mathbf{u} = \lambda \begin{pmatrix} 1 & 0 \\ 0 & -1 \end{pmatrix} \mathbf{u}$. This equation has only one linearly independent eigenvector $\mathbf{u} = \begin{pmatrix} 1 \\ -1 \end{pmatrix}$ and

$$\mathbf{u}^T \begin{pmatrix} 2 & 1 \\ 1 & 0 \end{pmatrix} \mathbf{u} = 0.$$

Accordingly, we should carefully normalize eigenvectors when the equation does not satisfy the condition.

Appendix C: Reverse propagation type I

For reverse propagation in the same framework as that of forward propagation, we define a $4LM \times 1$ column vector Ψ'_k as

$$\Psi'_k = \begin{pmatrix} 0 & 1 \\ 1 & 0 \end{pmatrix} \Psi_k \quad \text{for } 2N \geq k \geq 0.$$

The $4LM \times 4LM$ transfer matrix \mathbf{T}'_k , which satisfies $\Psi'_k = \mathbf{T}'_k \Psi'_{k+1}$, is defined as

$$\mathbf{T}'_{2N-1} = \begin{pmatrix} \frac{i\mathbf{M}_{tEH}\mathbf{U}_t}{h_t^2} \frac{1}{1-\theta_t} & \frac{i\mathbf{M}_{tEH}\mathbf{U}_t}{h_t^2} \frac{1}{1-\theta_t^{-1}} \\ \mathbf{U}_t & \mathbf{U}_t \end{pmatrix},$$

for $N > n \geq 1$,

$$\mathbf{T}'_{2n} = \begin{pmatrix} \mathbf{0} & \mathbf{1} \\ \frac{h_1(n)}{h_1(n-1)} & \frac{-i\mathbf{M}_{EH}(n)}{h_1(n-1)h_0(n)} \end{pmatrix},$$

$$\mathbf{T}'_{2n-1} = \begin{pmatrix} \mathbf{0} & \mathbf{1} \\ \frac{h_0(n)}{h_0(n-1)} & \frac{-i\mathbf{M}_{HE}(n-1)}{h_0(n-1)h_1(n-1)} \end{pmatrix},$$

and

$$\mathbf{T}'_0 = \begin{pmatrix} -ih_b^2(1-\theta_b) & \mathbf{U}_b^T & \mathbf{0} \\ ih_b^2\mathbf{U}_b(1-\theta_b) & \mathbf{U}_b^T & \mathbf{1} \end{pmatrix}.$$

The reverse equation corresponding to the forward Eq. (20) is

$$\begin{pmatrix} \hat{\mathbf{t}}' \\ \mathbf{0} \end{pmatrix} = \mathbf{T}'_0 \cdots \mathbf{T}'_{2N-1} \begin{pmatrix} \mathbf{1} \\ \hat{\mathbf{r}}' \end{pmatrix}.$$

Reverse iteration is defined as

$$\mathbf{C}'_k = \mathbf{T}'_k \mathbf{C}'_{k+1} \mathbf{P}'_k,$$

$$\mathbf{D}'_k = \mathbf{D}'_{k+1} \mathbf{P}'_k \quad \text{for } 0 \leq k \leq 2N-1,$$

with initial conditions,

$$\mathbf{C}'_{2N} = \begin{pmatrix} \mathbf{1} & \mathbf{0} \\ \mathbf{0} & \mathbf{1} \end{pmatrix} \quad \text{and} \quad \mathbf{D}'_{2N} = \begin{pmatrix} \mathbf{0} & \mathbf{1} \end{pmatrix}.$$

The column operator \mathbf{P}'_k can be defined in the same manner as Eq. (23); that is,

$$\mathbf{P}'_k = \begin{pmatrix} \mathbf{1} \\ -\frac{\mathbf{1}}{\mathbf{T}'_{k,10}\mathbf{C}'_{k+1,01} + \mathbf{T}'_{k,11}} \mathbf{T}'_{k,10} \mathbf{C}'_{k+1,00} \\ \frac{\mathbf{0}}{\mathbf{T}'_{k,10}\mathbf{C}'_{k+1,01} + \mathbf{T}'_{k,11}} \end{pmatrix},$$

without $k = 2N-1, 1$. \mathbf{P}'_{2N-1} and \mathbf{P}'_1 are

$$\mathbf{P}'_{2N-1} = \mathbf{P}'_1 = \begin{pmatrix} \mathbf{1} & \mathbf{0} \\ \mathbf{0} & \mathbf{1} \end{pmatrix},$$

because $\mathbf{T}'_{2N-1}(\mathbf{T}'_0)$ is different from $\mathbf{T}_0(\mathbf{T}_{2N-1})$. Here,

$$\mathbf{T}'_{2N-2} \mathbf{C}'_{2N-1} = \mathbf{T}'_{2N-2} \mathbf{T}'_{2N-1}$$

$$= \begin{pmatrix} \mathbf{U}_t & \mathbf{U}_t \\ \frac{-i\mathbf{M}_{tEH}\mathbf{U}_t}{h_1(N-2)h_t} \frac{1}{1-\theta_t^{-1}} & \frac{-i\mathbf{M}_{tEH}\mathbf{U}_t}{h_1(N-2)h_t} \frac{1}{1-\theta_t} \end{pmatrix}.$$

Thus,

$$\mathbf{P}'_{2N-2} = \begin{pmatrix} \mathbf{1} & \mathbf{0} \\ \theta_t & i(1-\theta_t)h_1(N-2)h_t\mathbf{U}_t^T \end{pmatrix}$$

and

$$\mathbf{C}'_{2N-2} = \mathbf{T}'_{2N-2} \mathbf{C}'_{2N-1} \mathbf{P}'_{2N-2}$$

$$= \begin{pmatrix} \mathbf{U}_t(1+\theta_t) & ih_1(N-2)h_t\mathbf{U}_t(1-\theta_t)\mathbf{U}_t^T \\ \mathbf{0} & \mathbf{1} \end{pmatrix}.$$

Furthermore,

$$\begin{aligned} \mathbf{C}'_1 &= \mathbf{T}'_1 \begin{pmatrix} \mathbf{C}'_{2,00} & \mathbf{C}'_{2,01} \\ \mathbf{0} & \mathbf{1} \end{pmatrix} \mathbf{P}'_1 \\ &= \begin{pmatrix} \mathbf{0} & \mathbf{1} \\ \mathbf{C}'_{1,10} & \mathbf{C}'_{1,11} \end{pmatrix}. \end{aligned}$$

Thus,

$$\mathbf{T}'_0 \mathbf{C}'_1 = \begin{pmatrix} \mathbf{0} & -ih_b^2(1-\theta_b)\mathbf{U}_b^T \\ \mathbf{C}'_{1,10} & \mathbf{C}'_{1,11} + ih_b^2\mathbf{U}_b(1-\theta_b)\mathbf{U}_b^T \end{pmatrix}.$$

From Eqs. (19), $\mathbf{T}'_0 \mathbf{C}'_1$ is an expression similar to $\mathbf{T}_{2N-1} \mathbf{C}_{2N-1}$. Reverse iteration yields

$$\hat{\mathbf{t}}' = \mathbf{C}'_{0,00} \quad \text{and} \quad \hat{\mathbf{r}}' = \mathbf{D}'_{0,10}.$$

At the n -th cell, we can introduce $\hat{\mathcal{E}}'(n, 2N-k)$ and $\hat{\mathcal{H}}'(n, 2N-k)$. For $1 \leq n \leq N-2$, the initial conditions are

$$\hat{\mathcal{E}}'(n, 2N-2n-2) = \hat{\mathcal{H}}'(n, 2N-2n-1) = \begin{pmatrix} \mathbf{0} & \mathbf{1} \end{pmatrix}.$$

The following iterations derive $\hat{\mathcal{E}}'(n, 2N)$ and $\hat{\mathcal{H}}'(n, 2N)$:

$$\begin{aligned} \hat{\mathcal{E}}'(n, 2N-k) &= \hat{\mathcal{E}}'(n, 2N-k-1) \mathbf{P}'_k \\ &\quad \text{for } 2n+1 \geq k \geq 0, \\ \hat{\mathcal{H}}'(n, 2N-k) &= \hat{\mathcal{H}}'(n, 2N-k-1) \mathbf{P}'_k \\ &\quad \text{for } 2n \geq k \geq 0. \end{aligned}$$

Appendix D: Reverse propagation type II

We can derive another equation for $\hat{\mathbf{r}}'$ and $\hat{\mathbf{t}}'$:

$$\begin{aligned} \begin{pmatrix} \hat{\mathbf{r}}' \\ \mathbf{0} \end{pmatrix} &= \mathbf{T}_{2N-1} \left[\mathbf{T}_{2N-2} \cdots \mathbf{T}_0 \begin{pmatrix} \mathbf{0} \\ \hat{\mathbf{t}}' \end{pmatrix} \right. \\ &\quad \left. - \begin{pmatrix} \mathbf{U}_t \\ \frac{i\mathbf{M}_{tEH}\mathbf{U}_t}{h_t^2} \frac{1}{1-\theta_t} \end{pmatrix} \right]. \end{aligned}$$

At the $2N-2 \rightarrow 2N-1$ step, we introduce \mathbf{C}'_{2N-1} and \mathbf{D}'_{2N-1} :

$$\begin{aligned} \mathbf{C}'_{2N-1} &= \begin{pmatrix} -\mathbf{U}_t + \mathbf{C}_{2N-1,01} \frac{i\mathbf{M}_{tEH}\mathbf{U}_t}{h_t^2} \frac{1}{1-\theta_t} \\ \mathbf{0} \\ \mathbf{C}_{2N-1,01} \\ \mathbf{1} \end{pmatrix}, \\ \mathbf{D}'_{2N-1} &= \begin{pmatrix} \mathbf{D}_{2N-1,01} \frac{i\mathbf{M}_{tEH}\mathbf{U}_t}{h_t^2} \frac{1}{1-\theta_t} & \mathbf{D}_{2N-1,01} \end{pmatrix}. \end{aligned}$$

Thus,

$$\mathbf{C}'_{2N} = \mathbf{T}_{2N-1} \mathbf{C}'_{2N-1} \mathbf{P}'_{2N-1}, \quad (\text{D1})$$

Note that $\mathbf{C}'_{k,01} = \mathbf{C}_{k,01}$, $\mathbf{D}'_{k,01} = \mathbf{D}_{k,01}$ and $\mathbf{P}'_{k,01} = \mathbf{P}_{k,01}$ for $2N-1 \leq k \leq 2N$. The iterative procedure of Eq. (D1) yields

$$\hat{\mathbf{r}}' = \mathbf{C}'_{2N,00} \quad \text{and} \quad \hat{\mathbf{t}}' = \mathbf{D}'_{2N,00}.$$

We can add $\hat{\mathcal{E}}'(n, 2N-1)$ and $\hat{\mathcal{H}}'(n, 2N-1)$ to the $2N-2 \rightarrow 2N-1$ step.

$$\begin{aligned} \hat{\mathcal{E}}'(n, 2N-1) &= \begin{pmatrix} \mathbf{0} & \hat{\mathcal{E}}_{01}(n, 2N-1) \end{pmatrix}, \\ \hat{\mathcal{H}}'(n, 2N-1) &= \begin{pmatrix} \mathbf{0} & \hat{\mathcal{H}}_{01}(n, 2N-1) \end{pmatrix}. \end{aligned}$$

Finally, we obtain

$$\begin{aligned} \hat{\mathcal{E}}'(n, 2N) &= \hat{\mathcal{E}}'(n, 2N-1) \mathbf{P}'_{2N-1}, \\ \hat{\mathcal{H}}'(n, 2N) &= \hat{\mathcal{H}}'(n, 2N-1) \mathbf{P}'_{2N-1}. \end{aligned}$$

-
- [1] J. D. Joannopoulos, S. G. Johnson, J. N. Winn, and R. D. Meade “Photonic Crystals,” 2nd-ed., Princeton University Press (2008).
 - [2] L. C. Kimerling, D. Ahn, A. B. Apsel, M. Beals, D. Carothers, Y.-K. Chen, T. Conway, D. M. Gill, M. Grove, C.-Y. Hong, M. Lipson, J. Liu, J. Michel, D. Pan, S. S. Patel, A. T. Pomerene, M. Rasras, D. K. Sparacin, K.-Y. Tu, A. E. White, and C. W. Wong, Proc. SPIE **6125**, 612502-1 (2006).
 - [3] D. A. B. Miller, Proc. IEEE **97**, 1166 (2009).
 - [4] A. Taflove, IEEE Transactions on Electromagnetic Compatibility, **EMC-22**, 191 (1980).
 - [5] Y. Urino, Y. Noguchi, M. Noguchi, M. Imai, M. Ya-

- magishi, S. Saitou, N. Hirayama, M. Takahashi, H. Takahashi, E. Saito, M. Okano, T. Shimizu, N. Hatori, M. Ishizaka, T. Yamamoto, T. Baba, T. Akagawa, S. Akiyama, T. Usuki, D. Okamoto, M. Miura, J. Fujikata, D. Shimura, H. Okayama, H. Yaegashi, T. Tsuchizawa, K. Yamada, M. Mori, T. Horikawa, T. Nakamura, and Y. Arakawa, Opt. Express **20**, B256 (2012).
- [6] T. Yamamoto, H. Kobayashi, M. Ekawa, S. Ogita, T. Fujii, T. Higashi and M. Kobayashi, Electronics Lett. **33**, 65 (1997).
- [7] Chapter 4 in A. Taflove and S. C. Hagness, “Computational Electrodynamics: The Finite-Difference Time-Domain Method,” 2nd-ed., Artech House (2000).

- [8] IEEE, “IEEE standard Floating-Point Arithmetic,” IEEE Std 754-2008, pp. 1-58, Aug 2008.
- [9] K. Cho, “Optical Response of Nano-structures: Microscopic Nonlocal Theory,” Springer Verlag, Heidelberg (2003); Errata, Web site of Springer Verlag for this book.
- [10] J. A. Wheeler, Phys. Rev. **52**, 1107 (1937).
- [11] M. Büttiker, Y. Imry, R. Landauer, and S. Pinhas, Phys. Rev. B **31**, 6207 (1985).
- [12] S. G. Tikhodeev, A. L. Yablonskii, E. A. Muljarov, N. A. Gippius, and T. Ishihara, Phys. Rev. B **66**, 045102 (2002).
- [13] Z.-Y. Li and L.-L. Lin, Phys. Rev. E **67**, 046607 (2003).
- [14] M. Liscidini, D. Gerace, L. C. Andreani, and J. E. Sipe, Phys. Rev. B **77**, 035324 (2008).
- [15] N. Anttu and H. Q. Xu, Phys. Rev. B **83**, 165431 (2011).
- [16] T. Usuki, M. Saito, M. Takatsu, R. A. Kiehl, and N. Yokoyama, Phys. Rev. B **52**, 8244 (1995).
- [17] R. Akis and D. Ferry, J. Comput. Electron. **9**, 232 (2010).
- [18] K. S. Yee, IEEE Trans. Antennas Propag. **AP-14**, 302 (1966).
- [19] Equation (1.44) and Fig. 2.11 in K. Okamoto, “Fundamentals of Optical Waveguides,” 2nd-ed., Elsevier Inc. (2006).
- [20] D. Y. K. Ko and J. C. Inkson, Phys. Rev. B **38**, 9945 (1988).
- [21] T. Usuki, M. Takatsu, R. A. Kiehl, and N. Yokoyama, Phys. Rev. B **50**, 7615 (1994).
- [22] S. Akiyama, T. Baba, M. Imai, T. Akagawa, M. Takahashi, N. Hirayama, H. Takahashi, Y. Noguchi, H. Okayama, T. Horikawa, and T. Usuki Opt. Express **20**, 2911 (2012).
- [23] Equations (6) and (7) in L. Tong, J. Lou, and E. Mazur, Opt. Express **12**, 1025 (2004).
- [24] “ITU-T G.694.2,” <http://www.itu.int/rec/T-REC-G.694.2-200312-I/e>
- [25] R. A. Soref, and B. R. Bennett, IEEE J. Quantum Electron., **QE23**, 123 (1987).
- [26] G. T. Reed, G. Mashanovich, F. Y. Gardes and D. J. Thomson, nature photonics **4**, 518 (2010).
- [27] E. Shiles, T. Sasaki, M. Inokuti and D. Y. Smith, Phys. Rev. B **22**, 1612 (1980).
- [28] Table 1 in M.A. Ordal, L. L. Long, R. J. Bell, S. E. Bell, R. R. Bell, R. W. Alexander, Jr. and C. A. Ward, Appl. Opt. **22**, 1099 (1983).